U. of Iowa 75-3

Department of Physics and Astronomy
THE UNIVERSITY OF IOWA
Iowa City, Iowa 52242

U. of Iowa 75-3

Angular Distributions of Electrons of Energy $E_e > 0.06$ MeV in the Jovian Magnetosphere

by

D. D. SENTMAN and J. A. VAN ALLEN

Department of Physics and Astronomy
The University of Iowa
Iowa City, Iowa 52242

January 1975

ABSTRACT

Results of an angular distribution analysis of electron intensity data recorded by the University of Iowa experiment aboard Pioneer 10 are presented for the Jupiter encounter period 26 November through 14 December 1973. The data were from three directional particle detectors with effective integral energy thresholds of E_e = 0.06, 0.55, and 5.0 MeV, respectively. It is found that the central core of the magnetosphere for radial distances less than 12 Jovian radii (R_J) is dominated by pitch angle distributions strongly peaked at $\alpha = 90°$, while the region of radial distances 12-25 R_J shows bidirectional and approximately equal maxima at $\alpha = 0°$ and 180°. Bidirectional angular distributions in the magnetodisc out to the radius of the magnetopause strongly suggest quasi-trapping on closed field lines as the predominant situation. Substantial field aligned, unidirectional streaming was detected on only two occasions each of about one hour's duration; one of these episodes immediately preceded the return of particle count rates to near interplenatary values for three hours on 1 December. No distinctive effects on angular distributions were discerned near the L-shells of satellites. Some interpretative suggestions are made.

I. INTRODUCTION

This paper reports on angular distributions of electrons of energy $E_e > 0.06$ MeV as observed during the December 1973 Jupiter encounter by the University of Iowa particle detectors on the Pioneer 10 spacecraft.

Preliminary and later, more thorough, reports [Fillius and McIlwain, 1974a, b; Simpson et al., 1974a, b; Trainor et al., 1974a, b; Van Allen et al., 1974a, b] showed that the outer magnetosphere of Jupiter consists of a relatively thin quasi-trapping region (magnetodisc) confined approximately to the magnetic equatorial plane and extending outward to more than 100 R_J (Jovian equatorial radii). Because of the ~ 10° tilt of the planet's magnetic dipole axis to its rotational axis [Smith et al., 1974a, b] the magnetic equator wobbles up and down with a period equal to the 10-hour planetary rotational period, giving the outer magnetosphere the appearance of a "flopping disc" to a stationary observer.

The angular distributions of charged particles give valuable clues as to the mechanisms responsible for the observed properties of the Jovian magnetosphere. Preliminary analysis [Van Allen et al., 1974b; Trainor et al., 1974b] showed that the predominant form for low-energy electron angular distributions in

the outer magnetosphere is one of approximate isotropy, with weak anisotropies appearing in the dayside region 60-90 R_J. These angular distributions were taken as evidence for closed field lines and quasi-trapping of energetic particles in the magnetodisc. Some examples of strong field-aligned, bidirectional anisotropies were reported at intermediate distances ($\sim$25 R_J) by Trainor et al. [1974a, b], Fillius and McIlwain [1974b], and Van Allen et al. [1974b]. Inside 12 R_J distributions peaked at pitch angles of 90° for electrons $E_e > 21$ MeV were inferred from the latitude dependence of omnidirectional intensities by Van Allen et al. [1974a, b] in general agreement with radioastronomical observations of the decimetric synchrotron radiation.

Prior particle species identification has shown that electrons are responsible for the large majority of particle counts recorded by the University of Iowa directional detectors during the Jupiter encounter [Van Allen et al., 1974b]. The present study presents the results of a systematic analysis of angular distributions of these particles for the entire encounter period beginning on DOY (Day of Year) 330/1973 and continuing through DOY 348. The analysis includes corrections for distribution distortion by rapidly varying fluxes, a search for magnetic field-aligned particle streaming and a rough classification of pitch angle distributions according to the existence, type, and strength of the associated anisotropies.

The magnetic field data used in this work were kindly supplied by E. J. Smith et al. of the Pioneer 10 magnetometer team.

II. INSTRUMENT

The University of Iowa instrument includes three directional detector systems, denoted by the letters G, B, and A, with electron effective integral response thresholds of 0.06 MeV, 0.55 MeV, and 5 MeV, respectively. Detectors B and A consist of EON Corporation end window type 6213 Geiger-Mueller tubes with physical shielding arranged so as to provide collimated, nearly unidirectional angular sensitivity cones. Detector G is also a 6213, but it is arranged in a scatter geometry in order to admit low-energy electrons preferentially and exclude protons $E_p < 20$ MeV.

Figure 1 shows the physical arrangement of the detectors and their associated angular sensitivity cones referred to a rectangular coordinate system fixed to the rotating spacecraft. The +Z axis is parallel to the spacecraft spin axis, and the three detector "look" axes are parallel to the +X axis. The +Y axis is chosen to make the coordinate system right-handed. The +Z axis of the spacecraft is pointed continuously toward the earth with an uncertainty of less than 1° and is therefore approximately parallel to the ecliptic plane. The sensitivity cones of the respective detectors are azimuthally symmetric about their central axes, with full-width, half-max angular diameters of ~ 42° for G and ~ 32°

for both B and A. Additional information on physical construction and calibration is given by Baker [1973] and Van Allen et al. [1974b].

The range of particle pitch angles available to the directional detectors depends on the orientation of the instantaneous magnetic field vector relative to the spacecraft spin axis. Figure 2 depicts the relevant geometry in terms of a spacecraft-centered, inertially-oriented coordinate system whose Z' axis is parallel to the spin axis and whose X' axis is parallel to the ecliptic plane (i.e., the ascending node of the spacecraft equatorial plane on the ecliptic). The instantaneous direction of the magnetic field vector is specified by the polar angle θ_B and roll angle φ_B.

In the accompanying analysis θ_B is used for determining pitch angle coverage. For this purpose the acute angle that the magnetic field makes with the spin axis is sufficient. Accordingly, θ_B will refer to that quantity. The angles θ_B and φ_B will be called the magnetic cone angle and magnetic clock angle, respectively.

As the spacecraft rotates, the axes of the detectors' sensitivity cones sweep around the unit sphere in the X'Y' plane of Figure 2. Hence, they sweep through the range of pitch angles α to the magnetic vector $(90° - \theta_B)$ to $(90° + \theta_B)$. The pitch angle 90° is crossed twice per spin but angles near 0° and 180° are often not viewed even in the edges of the fields of view.

The accuracy with which spin-averaged counting rates represent true omnidirectional fluxes is a function of both anisotropy strength and the completeness of pitch angle coverage. In the case of field-aligned bidirectional anisotropy and of small θ_B, a spin-average does not include the greatest intensities and is less than a true omnidirectional average intensity. In the case of angular distributions having a maximum at $\alpha = 90°$ and of small θ_B the spin average intensity is greater than the true omnidirectional average. In either case the observed angular distribution is more nearly isotropic than the true one, which is observed only for $\theta_B = 90°$. Because of the above effects, variability in the pitch angle coverage in the presence of strong particle anisotropies produces a correlated variability in the spin-averaged intensities. Occasions arise when small scale temporal structure in detector count rates are apparently attributable directly to changes in θ_B. For a large fraction of our observations θ_B is sufficiently close to 90° to assure that both the nature of the observed angular distributions and the spin averages are essentially valid.

III. ANALYSIS OF DATA AND ASSEMBLY OF ANGULAR DISTRIBUTIONS

Particle counts from each detector channel are accumulated for periods of time and at intervals dependent on the telemetry format and bit rate. During most of the Jovian encounter the telemetry rate was 1024 bps and the format was D/B, thus providing an accumulation time of 0.375 sec. During this period of time, there occurs a rotational displacement of 10°.7 at the spacecraft rotational period of 12.62 sec. The spacecraft roll angle assigned to a data sample is referenced to the fixed X' axis of Figure 2 at the mid-time of the sample. The interval between successive samples of a given detector was 4.125 sec, which corresponds to 117°.7 of rotational angle.

A relationship important to the discussion that follows is that between spacecraft spin period and the detector sampling interval. Figure 3 represents the angular sampling scheme in use during the major part of the encounter. If a sample is taken at point 1 initially, then subsequent samples are taken at 2, 3, and 4. Because the rotation sample interval $\delta = 117°.7$ is not a submultiple of 360°, positions 4 and 1 are separated by an angle of $\beta = 7°$.

The total time needed to sample all directions in angular steps of 7° is therefore $T \approx (\delta/\beta) \times (3 \text{ sample periods}) \approx 3.5$ min.

Strong bidirectional anisotropies are sampled in the direction of maximum intensity approximately every third sample with the direction of maximum intensity apparently reversing by 180° every 1.75 min, or twice within 3.5 min. This apparent switching in the time domain is an artifact of the sampling parameters prevailing at the time the data were taken. We have avoided the pitfalls of this effect by adopting 3.5 min as the basic analysis interval for assembling angular distributions.

Because of the nature of the sampling scheme described above it is apparent that in the presence of anisotropies the frame-by-frame detector data will show a spin modulation of period approximately equal to the spacecraft spin period. The information determining the relative degree of anisotropy is contained in the relative amplitude of the spin modulation. Hence a distorting effect on the angular distributions occurs if during the 3.5 min analysis interval the absolute omnidirectionally averaged intensity undergoes a change that is comparable to or larger than the absolute modulation amplitude. Such structure in the spin averages, with scale times on the order of minutes, is commonly observed in the detector data.

If it is assumed that the type of angular distribution and degree of anisotropy remain constant during the accumulation time needed to construct a complete distribution, distortion arising from intensity changes can be reduced considerably by a normalization

procedure. Dividing each sampled counting rate by the corresponding spin average defined over a suitable interval reduces the mean counting rate to unity but preserves the relative amplitude of the 12-sec spin modulation.

Figure 4 illustrates the normalization procedure. The instantaneous spin average is determined by smoothing the frame-by-frame data with an 11-point smoothing function with weights proportional to the tenth-order binomial coefficients to provide proper filter characteristics. A relatively distortion-free data set along with the associated normalized data (upper left, Figure 4) is shown with the corresponding angular distributions constructed therefrom (upper right, Figure 4). A more typical example of data obtained during encounter is similarly shown in the lower panels of Figure 4. In this and other figures the time shown is the universal time of reception of the Pioneer 10 data at the earth, designated Earth Received Time (ERT).

Once the data are normalized as described above an angular distribution is constructed for each detector by accumulating samples into angular bins of width 10° centered on multiples of 10° until each bin contains at least one data sample ($\approx$3.5 min). The resulting normalized distribution is then multiplied by the average value of the corresponding prenormalized data set.

For an initial survey of particle distributions observed during the encounter, the present analysis will be restricted to

the identification and parameterization of pitch angle anisotropies of the first and second orders. First order anisotropies correspond to distributions for which a measurable amount of unidirectional field-aligned particle streaming is present. Second order anisotropies are classified into two types, commonly called "dumb-bell" and "pancake". The former type of distribution corresponds to bidirectional field-aligned streaming with maximums at $\alpha = 0°$ and 180° while the latter has a maximum at $\alpha = 90°$.

The degree to which the detector data exhibit unidirectional streaming (first order anisotropy) is determined by constructing a dimensionless streaming index S for each of the normalized data sets. This index is defined as the difference between the positive flux and the negative flux through a unit area perpendicular to the local magnetic field vector $\vec{B}$ divided by the sum of these two fluxes. The sense is such that net streaming in the $+\vec{B}$ direction yields a positive value for S. The value of S lies between +1 and -1.

In order to determine the type of second-order pitch angle anisotropy (pancake or dumbbell) a Fourier fit is made to the normalized angular distribution using the expression

$$f(\varphi) = M [1 + K \cos 2 (\varphi - \Delta)]$$

where φ is the roll angle of a given detector's axis measured from the X' axis of Figure 2 in the sense of spacecraft rotation, $f(\varphi)$ is the roll angle distribution of counting rate, M is the spin-averaged counting rate, K is the modulation index (taken to be intrinsically positive), and Δ is the phase of the roll angle distribution. The angle Δ is taken to be modulo 180°; $f(\varphi)$ has maximums at $\varphi = \Delta$, and $\varphi = \Delta + 180°$.

The phase angle Δ determined by this fitting procedure is compared to the magnetic clock angle φ_B to determine which, if either, of the second order anisotropies is being observed. By reference to Figure 2, it is seen that maximum counting rates for dumbbell distributions occur for $\varphi = \varphi_B$ and $\varphi = \varphi_B + 180°$ whereas maximum counting rates for pancake distributions occur for $\varphi = \varphi_B \pm 90°$. Figure 4, for example, shows dumbbell distributions. The quantity $(\varphi_B - \Delta)$ therefore has values near 0° or 180° for dumbbell distributions; has values near 90° or 270° for pancake distributions; and is randomly distributed in angle for isotropic distributions. The quantity $(\varphi_B - \Delta)$ is computed for each complete normalized angular distribution data set of approximately 3.5 min duration.

It is noted that the streaming index for unnormalized data is moderately affected by the angular distribution distortion resulting from rapid intensity changes. On the other hand, the

phase angle Δ determined by harmonic analysis is only slightly affected by such distortions.

All counting rate data used in this study have been corrected for dead-time effects [Van Allen et al., 1974b].

IV. OBSERVED ANGULAR DISTRIBUTIONS

A. The Outer Magnetosphere $R \geq 25\ R_J$

1. Inbound

After the initial bow shock crossing and prior to the magnetopause crossing on the sunward side of Jupiter at 2038 ERT/DOY 331 (i.e., for radial distances greater than 97 R_J) essential isotropy was observed in all three detectors. Immediately after leaving the magnetic disorder of the magnetosheath and entering the comparatively ordered magnetodisc region, 5-10% anisotropies (100 K) of pancake type appeared in detector G distributions. This weak anisotropy slowly relaxed until about 0400 ERT/DOY 332, at which time the distributions became isotropic. The detectors of more energetic electrons, B and A, showed no anisotropies during this period. The acute magnetic cone angle θ_B stayed in the range 50-70° throughout this region.

Beginning at about 0500 ERT/DOY 332 dumbbell distributions appeared in the data for both detectors G and B, but not for A. These anisotropies, with a persistent strength of 10-20%, lasted until 0500 ERT/DOY 333. θ_B for this region stretching inward from 92 R_J to about 80 R_J was generally 80-90° with short

intervals near the ends of the period having $\theta_B \approx 70°$. Thus nearly complete pitch angle coverage was achieved. Figure 5 shows sample angular distributions for detectors G and B taken following the magnetopause crossing and at 86 R_J, respectively.

From about 0500 ERT/DOY 333 up to and including the "dropout" period early on DOY 335 essentially isotropic conditions prevailed, with occasional short bursts of anisotropic behavior. Two such events, the only episodes of significant unidirectional field-aligned particle streaming observed during the entire encounter period, are depicted in Figure 6. The streaming index S for detector G and the magnetic cone and clock angles are plotted, with the particle distributions at the times of peak streaming shown as insets.

The streaming example shown in the right-hand part of Figure 6 occurred during the period starting at the onset of declining counting rates which signaled the start of the dropout early on DOY 335 and continued until nearly interplanetary rates prevailed. It is not observed to coincide with any large changes in either field strength or direction.

The streaming that occurred during a period of approximately one hour duration on DOY 334 (left-hand plot in Figure 6) at a distance of 65 R_J is observed to coincide with marked changes in the magnetic field direction. Such streaming may be a result of locally induced electric fields. Alternately, it could be the

effect of the intermittent opening and closing of field lines from a centrifugally induced tearing away of part of the magnetodisc.

At about 2300 ERT/DOY 335, immediately after the reestablishment of the particle fluxes following the dropout, moderately weak (5-15%) but well defined pancake distributions appeared in the data from detectors G and B. By approximately 0400 ERT of the following day the distribution had changed to dumbbell, then returned to pancake at 0800 ERT.

Figure 7 shows a plot of the quantity $(\varphi_B - \Delta)$ for detector G during DOY 336, as well as other pertinent parameters helpful in interpreting the results (refer to Section III for definition and discussion of these parameters). In addition to considerable structural detail in several of the quantities plotted, an approximate ten-hour periodicity is seen in $(\varphi_B - \Delta)$. Recall that this quantity (which in this figure is modulo 180° and plotted on the interval (-45°, 135°)) will tend to have values near 0° for dumbbell distributions and 90° for pancakes.

The times of maximum northward magnetic latitude excursion for the inbound spacecraft in a dipole field tilted toward $\ell_{III} = 230°$ are indicated by solid arrows in the figure. At these times the spacecraft is on or near the magnetic equator. It is observed that when the sunward magnetospheric phase lead arising from magnetospheric distortion [Van Allen et al., 1974b; Northrop et al., 1974; McKibben and Simpson, 1974; Fillius and McIlwain, 1974b]

is taken into account the pitch angle distributions tend (with some exceptions) to be predominantly dumbbell on or near the distorted magnetic equator (dashed arrows) and mildly pancake at off equatorial latitudes. Although considerable variability in the magnetic cone angle θ_B severely limits the pitch angle coverage during some portions of this day, firm identification of the primary type of pitch angle distribution is not affected except for the last 4 hours of the day, during which there are large variations in Δ but the average tendency is toward dumbbells. It is suggested that dumbbell distributions correspond to more durably trapped particles on closed field lines near the central part of the magnetodisc, whereas pancake distributions (toward the lower surface of the magnetodisc) correspond to alternately open and closed field lines (with scattering) so that particle leakage occurs preferentially for particles having pitch angles near 0° or 180°. The further stage in this suggested hierarchy is unpopulated, open field lines above and below the magnetodisc.

Apparent correlations between the modulation index K, magnetic cone angle θ_B, and spin average M are evident in Figure 7. As previously suggested, some of the effects on K and M may be attributed to changes in θ_B. Two examples of the effects of rapid cone angle changes on the detector spin averages and apparent anisotropy strengths are shown in Figure 8. Both examples are taken from time periods when dumbbell pitch angle

distributions are observed. The strong correlation among the three quantities suggests that when strong anisotropies are present the small-scale structure in detector spin averages derives partially and perhaps dominantly from the incompleteness of the continuously changing pitch angle coverage.

2. Outbound

The dawnward side of the magnetodisc traversed during the outbound portion of encounter showed essentially isotropic distributions for all three directional detectors and at all distances beyond 25 R_J.

The only exceptions to this isotropy occurred during two brief intervals on DOY 340 when the spacecraft was experiencing the increased counting rates associated with momentary immersion into the current sheet believed to exist there [Smith et al., 1974b]. During both intervals the anisotropies appeared only in detector G and were of the dumbbell type. The first occurred from 0200-0530 ERT with anisotropy strengths in the range 5-10%. The second was from 1130-1700 ERT with variable anisotropy strengths as high as 30%.

The magnetic cone angle θ_B held relatively steady at 60-80° in the dawnside region from 25-90 R_J; hence the comparative absence of detectable anisotropies in the data conclusively establishes isotropic particle distributions in this region of the magnetosphere.

B. The Inner Magnetosphere $R \leq 25\ R_J$

The results of the angular distribution analysis for the inner region of the Jovian magnetosphere are summarized in Figures 9 through 12. These figures plot the quantities $(\varphi_B - \Delta)$, θ_B, M, and K as functions of time during DOY's 337 and 338 for each of the low-energy particle detectors G and B. The salient features of these plots are the following.

(1) $12 \leq R \leq 25\ R_J$. For both detectors, strong dumbbell anisotropies appear at 0100 ERT/DOY 337. Except for the indecisive period 0500-1000 ERT, these dumbbells last beyond 1400 ERT for detector B and 1600 ERT for detector G. Dumbbells are also dominant late on DOY 338 during the period 1900-2300 ERT. The strength of these second-order anisotropies, as measured by the index K, is seen to be apparently related to the magnetic cone angle θ_B. The period 0500-1000 ERT/DOY 337 shows relative isotropy for both detectors, as does the period 1500-1900 ERT the following day. The magnetic cone angle during these times is such as to provide restricted pitch angle coverage, suggesting that the apparent isotropy observed during these times may be due simply to the fact that bidirectional components with pitch angles near 0° and 180° are not being observed.

Reference to the meridional trace of the spacecraft encounter trajectory in magnetic dipole coordinates (Figure 13, the so-called

"wiggle diagram") sheds some light on the observed behavior of the distributions. At the times when the strongest dumbbells are observed, pitch angle coverage is complete and the spacecraft is nearest the magnetic equator in the region $12 \leq R \leq 25\ R_J$. It is suggested that such dumbbells might plausibly dominate this entire region. However, because the range of pitch angles scanned by the directional detectors circumstantially decreases with increasing magnetic latitude, the bidirectional lobes containing particles with small pitch angles become lost to the rotating detector fields of view. Such a loss of the detectable anisotropic component is believed to be primarily responsible for the apparent isotropy observed in the angular distributions during these times. An additional effect which contributes to the observed isotropy is the isotropization of magnetic equatorial dumbbell distributions as one moves to high magnetic latitudes along the field line on which the particles are trapped.

(2) $R \leq 12\ R_J$. The inner core region of the magnetosphere shows strong pancake pitch angle distributions for the measured low-energy electrons as evidenced in Figures 9 through 12. Starting from approximately 1600 ERT/DOY 337 and lasting until about 1300 ERT the following day, the quantity $(\varphi_B - \Delta)$ is, with several noted exceptions, more or less continuously near a value of 90°.

Two effects in the data leading to irregular apparent distributions during portions of this time period are noted. First, in

detector G it is seen that from 2000 ERT/DOY 337 to 1000 ERT/DOY 338, $(\varphi_B - \Delta)$ lies at a value nearly 40° larger than the 90° expected for a pancake distribution. A thorough analysis of this effect shows that it is the result of a significantly altered detector geometric factor and directionality of detector G for high energy electrons ($E_e \geq 20$ MeV) in the core region inside approximately 10 R_J. High-energy electrons penetrating an asymmetrically located "soft" spot in the shielding of detector G shift the sensitivity cone away from its normal position symmetric with the spacecraft X axis. This leads to an offset in the computed value of Δ, the angular distribution phase angle. The offset has an azimuthal magnitude of approximately +40° which corresponds well in both magnitude and direction with the results of calibration tests performed on detector G [Baker, 1973].

With the above instrumental effect taken qualitatively into account, the distributions for detector G are seen to be moderately strong pancakes throughout the inner magnetosphere.

This effect does not occur for detector B. However, another and different effect appears in the quantity $(\varphi_B - \Delta)$ for detector B during the period 2200 DOY 337 to 0800 DOY 338. The counting rates for this detector are such during this period of intense particle intensities that it is operating in a performance regime where it is relatively insensitive to large intensity changes. Such reduced resolution translates into an uncertain phase angle Δ for

the associated angular distributions and results in unreliable distribution identification. The time periods containing the data for which this condition occurs have therefore been deleted from Figures 11 and 12. After 0900 DOY 338 the lowered counting rates from detector B again allow firm phase measurements to be made.

With the above mentioned data effects taken into account it appears that electrons $E_e > 0.06$ MeV in the central region of the magnetosphere at distances of less than about 12 R_J have pitch angle distributions that are strongly pancake in character. A similar conclusion for the higher energy electrons $E_e > 21$ MeV has been inferred previously from the latitude dependence of the omnidirectional intensities of such particles [Van Allen et al., 1974b].

Finally, it is noted from Figures 9-12 that no clearly identifiable effects on the angular distributions of electrons are associated with passage through the magnetic shells of Ganymede, Europa, and Io.

V. SUMMARY OF OBSERVED ANGULAR DISTRIBUTIONS

The run of observations suggests the following summary of the spatial distribution of electron $E_e > 0.06$ MeV pitch angle distributions for the regions of the Jovian magnetosphere surveyed during the Pioneer 10 encounter.

(1) The inner core hard trapping region $R \leq 12\ R_J$ displays pitch angle distributions that are pancake in character for all measured low-energy electrons. These distributions are of the same type as those deduced previously for higher energy electrons ($E_e > 21$ MeV) in this region [Van Allen et al., 1974b; Simpson et al., 1974b; Fillius and McIlwain, 1974b].

(2) The region between 12 and 25 R_J shows strong field-aligned bidirectional anisotropies. The maximum strength of these anisotropies occurs at approximately $20 \pm 3\ R_J$. The lowest electron energies observed show the largest degree of anisotropy, while electrons with energies greater than about 5 MeV show very little of the anisotropic behavior prevalent at lower energies.

(3) The nature of electron pitch angle distributions in the outer magnetosphere $R \gtrsim 25\ R_J$ is dependent on local time and on effective magnetic latitude. Near the noon meridian at distances between ~ 25 and 40 R_J weak anisotropies show periodic behavior

corresponding to the 10-hour rotational period of the planet. The nature of the periodicities at this local time is such that dumbbells occur on or near the magnetic equator, while weak pancakes appear at off-equatorial latitudes. The distributions on the noonside of Jupiter at distances of 60-100 R_J show weak dumbbells (bidirectional). The occurrence and persistence of these anisotropies seem to show a correlation with the degree of disorderliness in the magnetic field, such as is displayed during DOY's 333 and 334. Two brief instances of unidirectional field-aligned streaming suggest the existence of dynamical processes in this region. Near the dawn meridian at distances greater than 25 R_J the particle distributions for each of the detected energies are predominantly isotropic. Exceptions to this isotropy occurred briefly for the lowest energy electrons at distances of about 40 R_J.

VI. INTERPRETATIVE REMARKS

The pancake distributions inside of 12 R_J are considered to be roughly analogous to those in the strong trapping regions of the terrestrial radiation belts. Presumably these distributions result from inward radial diffusion with approximate conservation of the first and second adiabatic invariants μ and J and from the inevitable existence of loss cones near $\alpha = 0°$ and 180°.

In quasi-trapping regions of the terrestrial magnetosphere, dumbbell distributions prevail [Haskell, 1969]. It is tempting to apply analogous considerations to the distributions in the Jovian magnetodisc, though we do not pretend to offer any full explanation of the observations.

The following further remarks are of a qualitative and descriptive nature.

(a) Isotropic and dumbbell distributions suggest quasi-trapping or durable trapping with a wide distribution of mirror points. The suggestion is stronger for dumbbell distributions. In neither case is it rigorous, because open field lines having kinks and many back-scattering centers can masquerade as closed field lines. An analysis of the magnetic field topology in the magnetodisc by the Euler potential technique does, however,

strongly indicate that magnetic field lines near the central plane of the magnetodisc are indeed closed, whereas the relatively unpopulated lines above and below the magnetodisc are open [Goertz et al., 1975].

(b) On the upper and lower faces of the magnetodisc (defined as the distant magnetospheric region populated by electrons $E_e > 0.06$ MeV), there is presumably a transition region of time-variable openness and closedness. Particles having pitch angles near 0° and 180° will leak out preferentially during transient openness, thus tending to produce pancake distributions, as observed. An illuminating example of such an effect occurred on DOY 331 immediately inside the sunward magnetopause (upper part of Figure 5). Another occurred on DOY 335 immediately following the particle intensity "dropout" on that day.

(c) Further local time and real-time effects on the angular distributions may be expected during the cyclic diurnal expansion and compression of the outer magnetosphere as well as during transient fluctuations induced by variable solar wind pressure.

(d) The possibility that the strong dumbbell distributions in the radial range 12-25 R_J might be a natural result of injection of low energy electrons at the magnetopause and subsequent inward diffusion in the much distended magnetodisc field has been investigated by a numerical experiment. For this purpose there was constructed a magnetic field model approximating the main

features of the distended field observed by Smith et al. [1974] on the dawn side of Jupiter. Particles with various pitch angles were injected at 50 R_J on the magnetic equator and imagined to diffuse inward under the conservation of the adiabatic invariants μ and J. The equatorial pitch angles of the particles were then numerically evaluated as a function of radial distance from Jupiter. The calculations showed that all particle pitch angles drifted toward 90° as the particles diffused toward the undistorted dipole field, even when the particles were in the severely distended region of the model. Therefore, pitch angle distributions comprising such particles should show a progressive increase at $\alpha = 90°$ and depletion at the ends of the distribution as inward diffusion proceeds. In particular, isotropic injection at 50 R_J should result in pancake distributions everywhere interior to this point if μ and J are conserved and if large scale electric fields are absent. Thus such a simple set of assumptions regarding particle diffusion conditions does <u>not</u> account for the observed dumbbell distributions at 20 R_J.

VII. ACKNOWLEDGEMENTS

Our basic general acknowledgements have been given in an earlier paper [Van Allen et al., 1974b]. The analysis of the present paper was strongly dependent on detailed magnetic field data, kindly made available to us by the Pioneer 10 magnetometer team via E. J. Smith of the Jet Propulsion Laboratory.

Our work has been supported in large part by Contract NAS2-6553 with the Ames Research Center of the National Aeronautics and Space Administration.

REFERENCES

Baker, D. N., Calibration of University of Iowa instruments aboard Pioneers F and G, M.S. thesis, University of Iowa, Iowa City, May 1973.

Fillius, R. W., and C. E. McIlwain, Radiation belts of Jupiter, Science, 183, 314-315, 1974a.

Fillius, R. W., and C. E. McIlwain, Measurements of the Jovian radiation belts, J. Geophys. Res., 79, 3589-3599, 1974b.

Goertz, C. K., B. A. Randall, and M. F. Thomsen, Private Communication, 1974.

Haskell, G. P., Anisotropic fluxes of energetic particles in the outer magnetosphere, J. Geophys. Res., 74, 1740-1748, 1969.

McKibben, R. B., and J. A. Simpson, Evidence from charged particle studies for the distortion of the Jovian magnetosphere, J. Geophys. Res., 79, 3545-3549, 1974.

Northrop, T. G., C. K. Goertz, and M. F. Thomsen, The magnetosphere of Jupiter as observed with Pioneer 10. Part 2. Nonrigid rotation of the magnetodisc, J. Geophys. Res., 79, 3579-3587, 1974.

Simpson, J. A., D. Hamilton, G. Lentz, R. B. McKibben, A. Mogro-Campero, M. Perkins, K. R. Pyle, A. J. Tuzzolino, and J. J. O'Gallagher, Protons and electrons in Jupiter's magnetic field: Results from the University of Chicago experiment on Pioneer 10, Science, 183, 306-309, 1974a.

Simpson, J. A., D. C. Hamilton, R. B. McKibben, A. Mogro-Campero, K. R. Pyle, and A. J. Tuzzolino, The protons and electrons trapped in the Jovian dipole magnetic field region and their interaction with Io, J. Geophys. Res., 79, 3522-3544, 1974b.

Smith, E. J., L. Davis, Jr., D. E. Jones, D. S. Colburn, P. J. Coleman, Jr., P. Dyal, and C. P. Sonett, Magnetic field of Jupiter and its interaction with the solar wind, Science, 183, 305-306, 1974a.

Smith, E. J., L. Davis, Jr., D. E. Jones, P. J. Coleman, Jr., D. S. Colburn, P. Dyal, C. P. Sonett, and A. M. A. Frandsen, The planetary magnetic field and magnetosphere of Jupiter: Pioneer 10, J. Geophys. Res., 79, 3501-3513, 1974b.

Trainor, J. H., B. J. Teegarden, D. E. Stilwell, F. B. McDonald, E. C. Roelof, and W. R. Webber, Energetic particle population in the Jovian magnetosphere: A preliminary note, Science, 183, 311-313, 1974a.

Trainor, J. H., F. B. McDonald, B. J. Teegarden, W. R. Webber, and E. C. Roelof, Energetic particles in the Jovian magnetosphere, J. Geophys. Res., 79, 3600-3613, 1974b.

Van Allen, J. A., D. N. Baker, B. A. Randall, M. F. Thomsen, D. D. Sentman, and H. R. Flindt, Energetic electrons in the magnetosphere of Jupiter, Science, 183, 309-311, 1974a.

Van Allen, J. A., D. N. Baker, B. A. Randall, and D. D. Sentman, The magnetosphere of Jupiter as observed with Pioneer 10, Part 1. Instrument and principal findings, J. Geophys. Res., 79, 3559-3577, 1974b.

FIGURE CAPTIONS

Figure 1. A sketch showing the physical orientation of the low-energy detectors in the University of Iowa instrument package in relation to the spacecraft coordinate system. The detector sensitivity cones are cylindrically symmetrical about axes which are parallel to the spacecraft X-axis.

Figure 2. A diagram defining θ_B and φ_B, the magnetic cone and clock angles, respectively. The X'Y'Z' cartesian coordinate system is spacecraft-centered, non-rotating.

Figure 3. The angular sampling scheme prevailing during the encounter period. The circle represents spacecraft roll angle, and the numbers label the roll angle at consecutive detector samples.

Figure 4. Examples of the effects of data normalization on representative data sets. The upper two panels show that, in the absence of significant angular distribution distortion arising from rapid time-changes in omnidirectional intensity, the normalization procedure faithfully reproduces the actual distribution. The lower two panels, constructed from data more representative of the encounter period, illustrate the relative improvement achieved in the angular distributions as a result of data normalization.

Figure 5. Sample angular distributions observed in the dayside region of the magnetosphere at large radial distances. The upper panel shows a typical pancake distribution obtained at 95 R_J immediately after the inbound magnetopause crossing. The lower panel shows a weak dumbbell distribution typical of those observed in the region 70-90 R_J. Both distributions are constructed from 15-min averages to improve counting statistics.

Figure 6. The two instances of unidirectional field-aligned streaming observed during encounter. The left-hand panel is constructed from data taken at about 65 R_J on the noonside of Jupiter. The right-hand panel shows the streaming associated with the dayside data dropout early on DOY 335. The insets show angular distributions at the indicated times, referenced to the projection of the local magnetic field onto the detector viewing plane.

Figure 7. Plot showing the 10-hour periodic behavior of the pitch angle distribution of electrons $E_e > 0.06$ MeV on DOY 336. The quantity $(\varphi_B - \Delta)$, the magnetic cone angle θ_B, the spin averaged counting rate M, and the modulation index K are plotted for each of the 3.5 min duration angular distributions constructed for the entire data day. The definition and discussion of each of these parameters are given in the text.

Figure 8. Two illustrations of the effects of a variable magnetic cone angle θ_B on the spin-averaged counting rate M and the modulation index K for data taken with detector G.

Figure 9. Plot similar to Figure 7 covering DOY 337 and showing the behavior of the pitch angle distributions observed with detector G.

Figure 10. Plot similar to Figure 9 covering DOY 338 and showing the behavior of the pitch angle distributions observed with detector G.

Figure 11. Plot for detector B similar to and covering most of the same time period as Figure 9.

Figure 12. Plot for detector B similar to and covering most of the same time period as Figure 10.

Figure 13. The time-labeled trace of Pioneer 10 on a magnetic meridian plane moving with the spacecraft. The Jovian dipole model as specified was empirically determined from high-energy electron counting rates. The cross hatched regions are cross sections of the L-shell volumes swept out by the respective Jovian satellites [after Van Allen et al., 1974b].

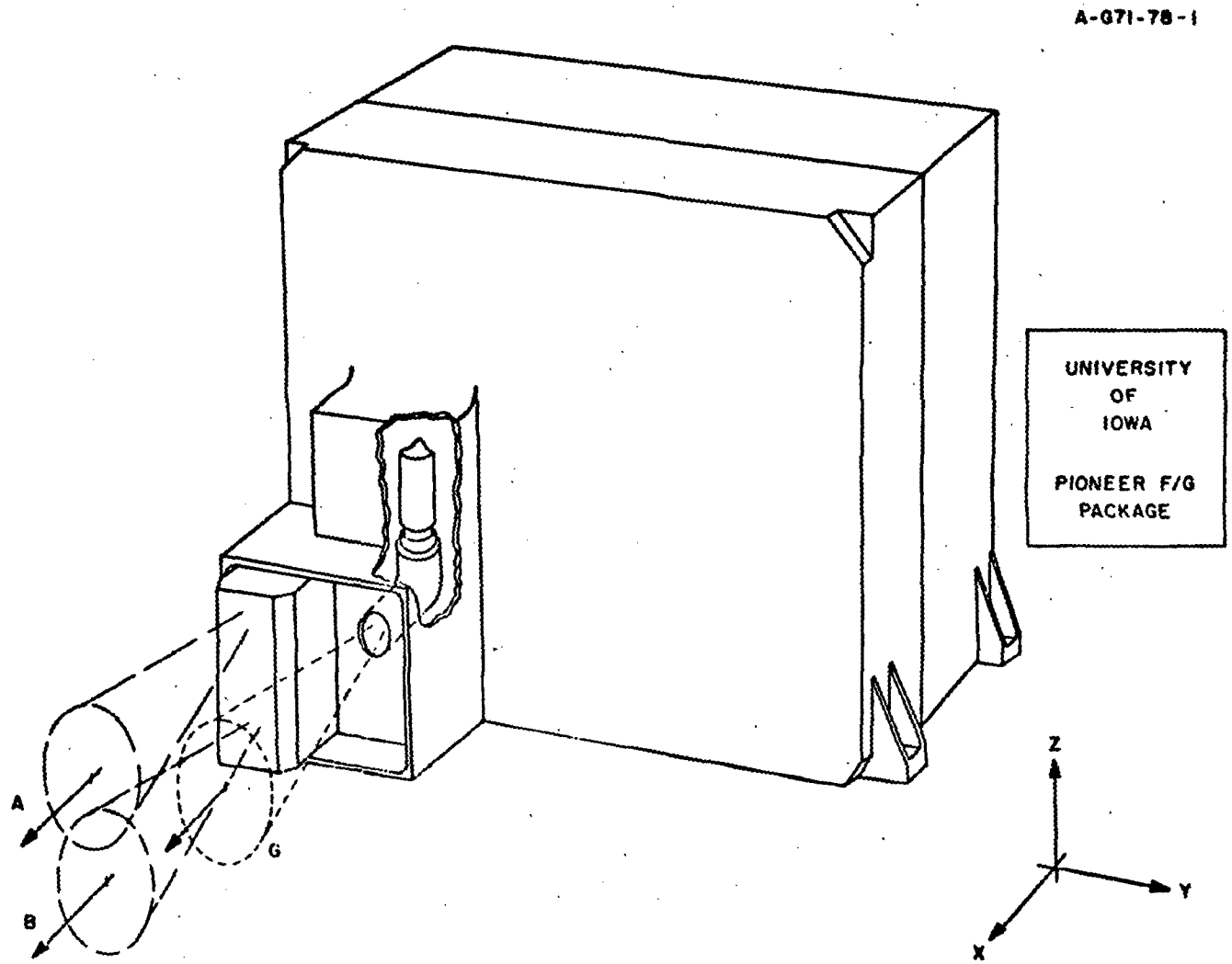

Figure 1

A-G74-632

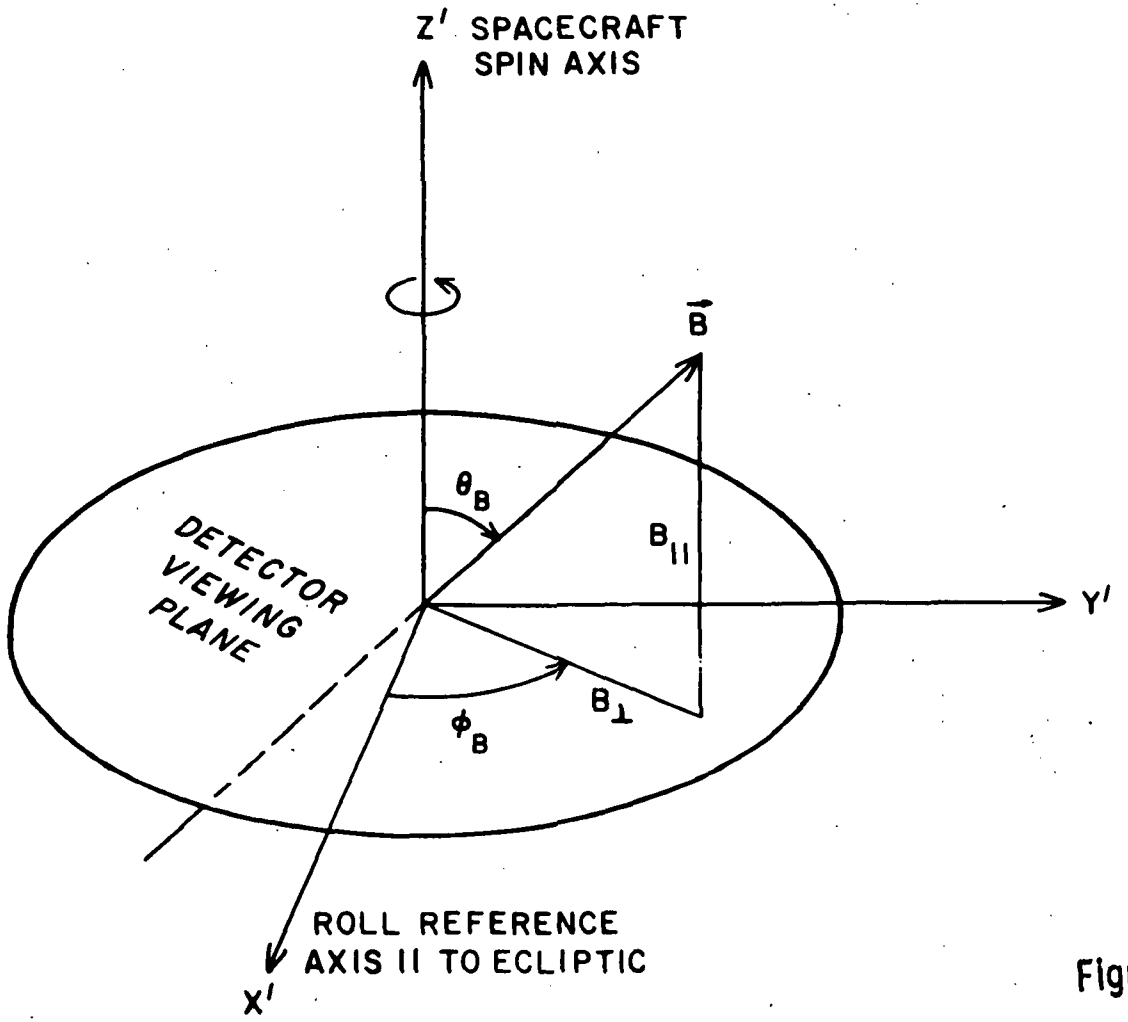

Figure 2

A-G74-879

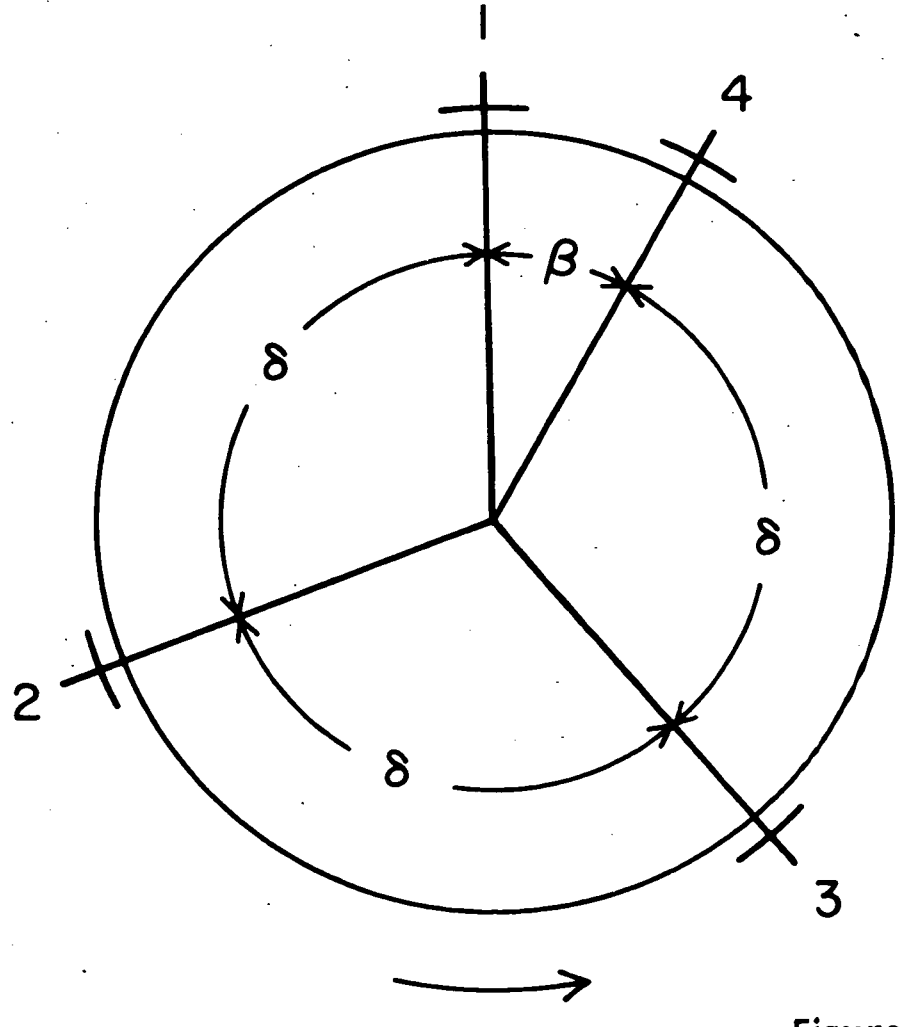

Figure 3

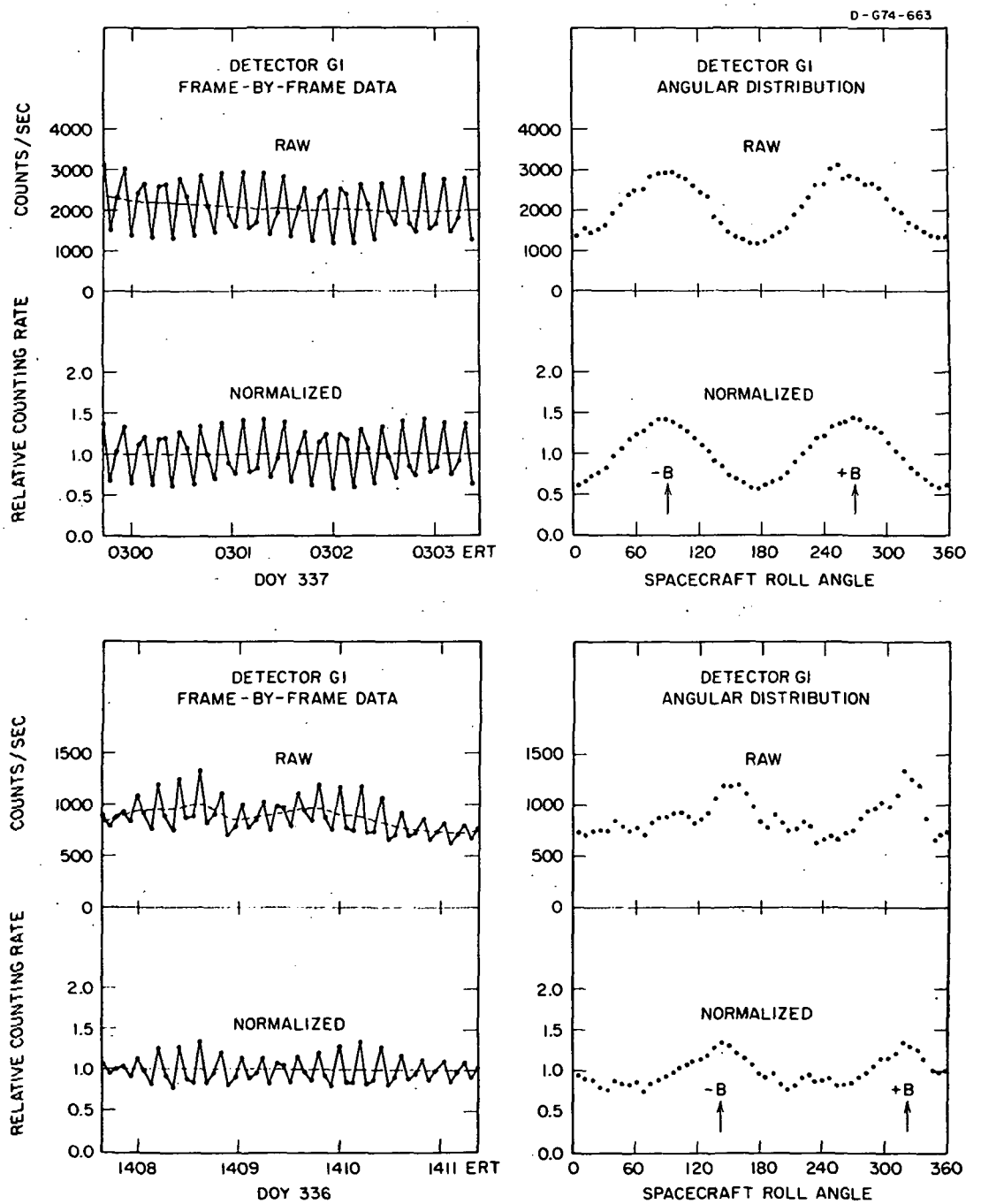
D-G74-663
DETECTOR G1
FRAME-BY-FRAME DATA
RAW
NORMALIZED
COUNTS/SEC
RELATIVE COUNTING RATE
4000
3000
2000
1000
0
2.0
1.5
1.0
0.5
0.0
0300
0301
0302
0303 ERT
DOY 337
DETECTOR G1
ANGULAR DISTRIBUTION
RAW
NORMALIZED
-B
+B
0
60
120
180
240
300
360
SPACECRAFT ROLL ANGLE
DETECTOR G1
FRAME-BY-FRAME DATA
RAW
NORMALIZED
COUNTS/SEC
RELATIVE COUNTING RATE
1500
1000
500
0
2.0
1.5
1.0
0.5
0.0
1408
1409
1410
1411 ERT
DOY 336
DETECTOR G1
ANGULAR DISTRIBUTION
RAW
NORMALIZED
-B
+B
0
60
120
180
240
300
360
SPACECRAFT ROLL ANGLE

Figure 4

B-G74-682-2

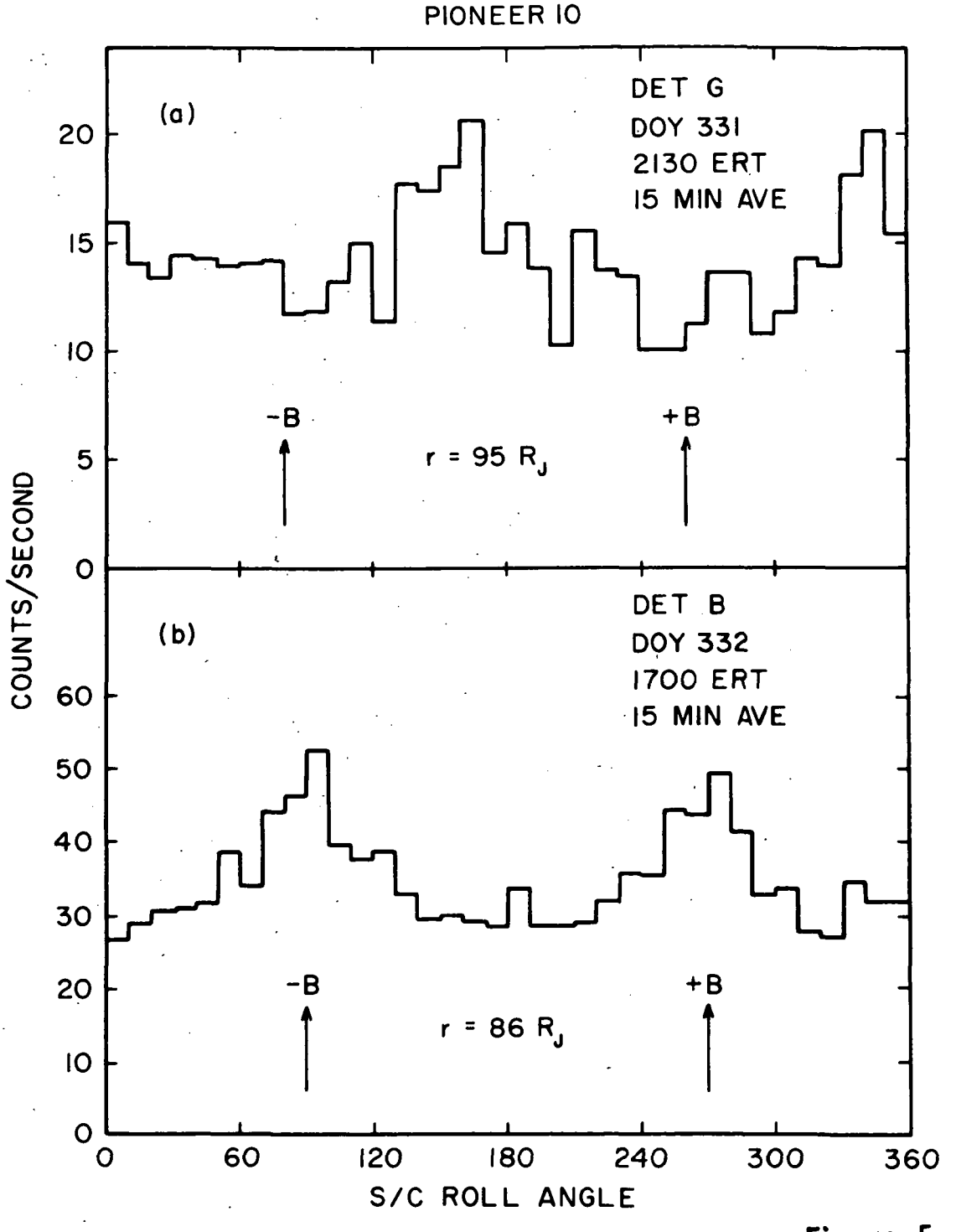

Figure 5

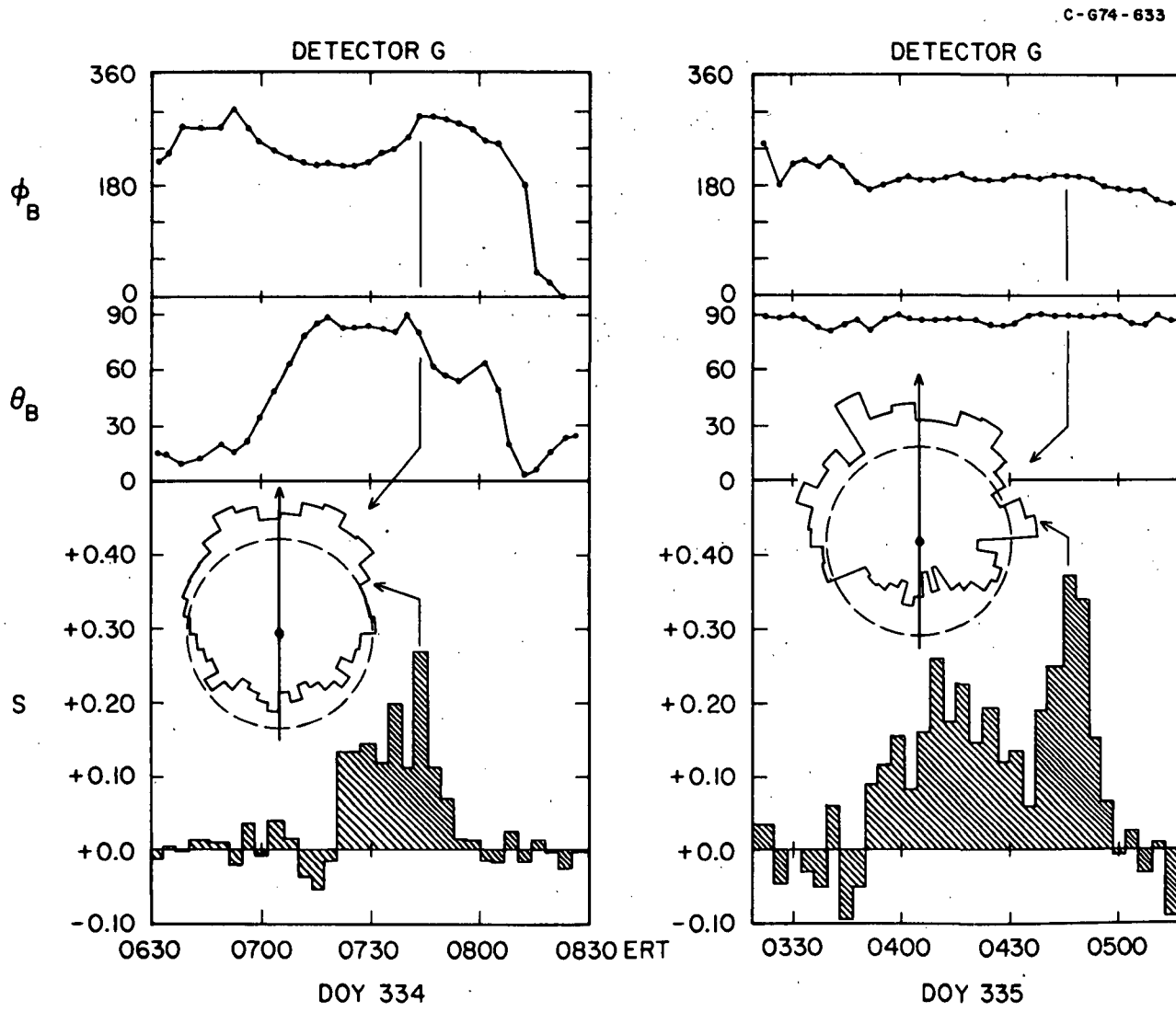
C-G74-633
DETECTOR G
DETECTOR G
ϕ_B
θ_B
S
360
180
0
90
60
30
0
+0.40
+0.30
+0.20
+0.10
+0.0
-0.10
0630
0700
0730
0800
0830 ERT
DOY 334
0330
0400
0430
0500
DOY 335

Figure 6

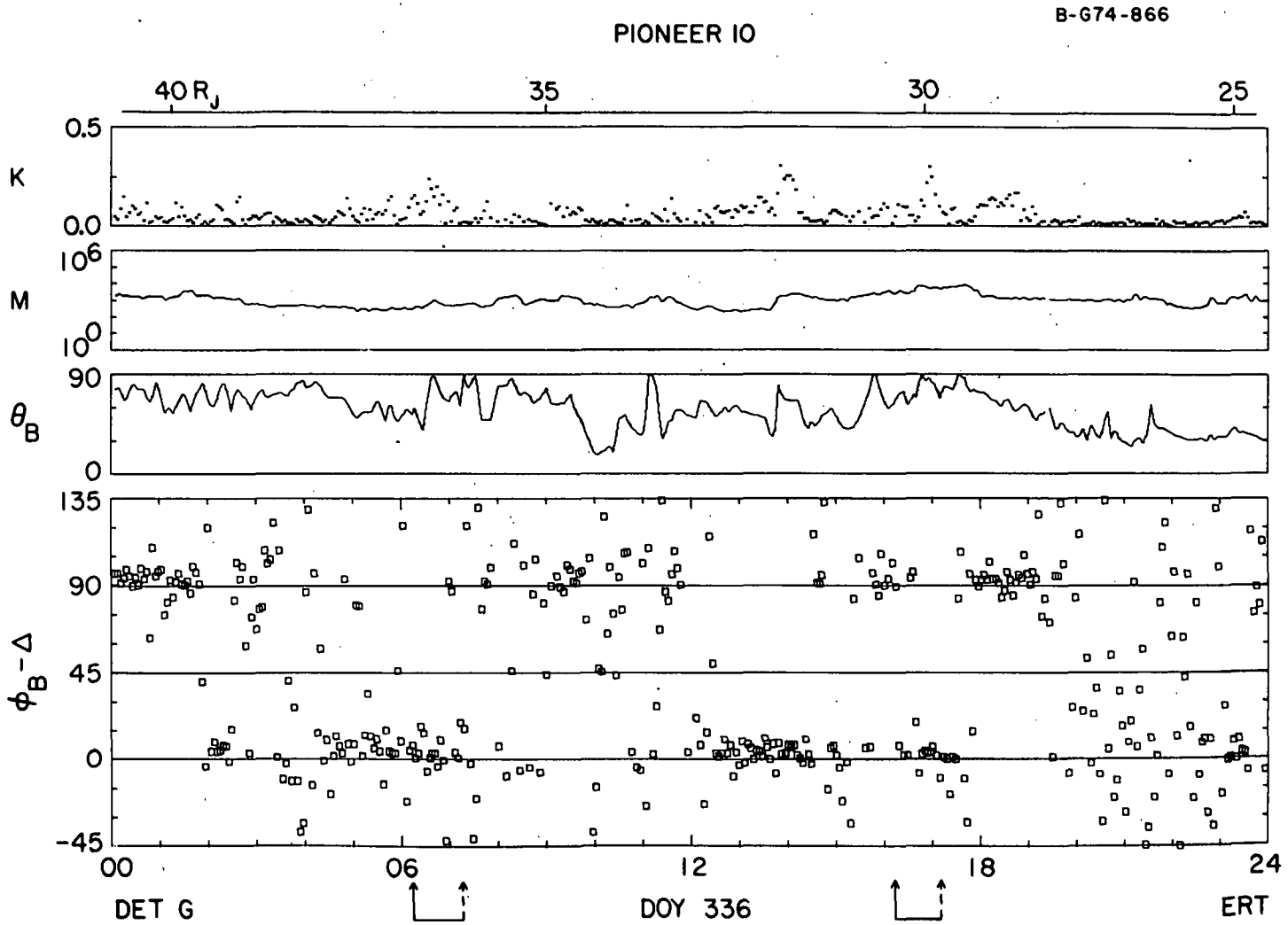
B-G74-866
PIONEER 10
40 R_J
35
30
25
0.5
K
0.0
10^6
M
10^0
90
θ_B
0
135
90
φ_B - Δ
45
0
-45
00
06
12
18
24
DET G
DOY 336
ERT

Figure 7

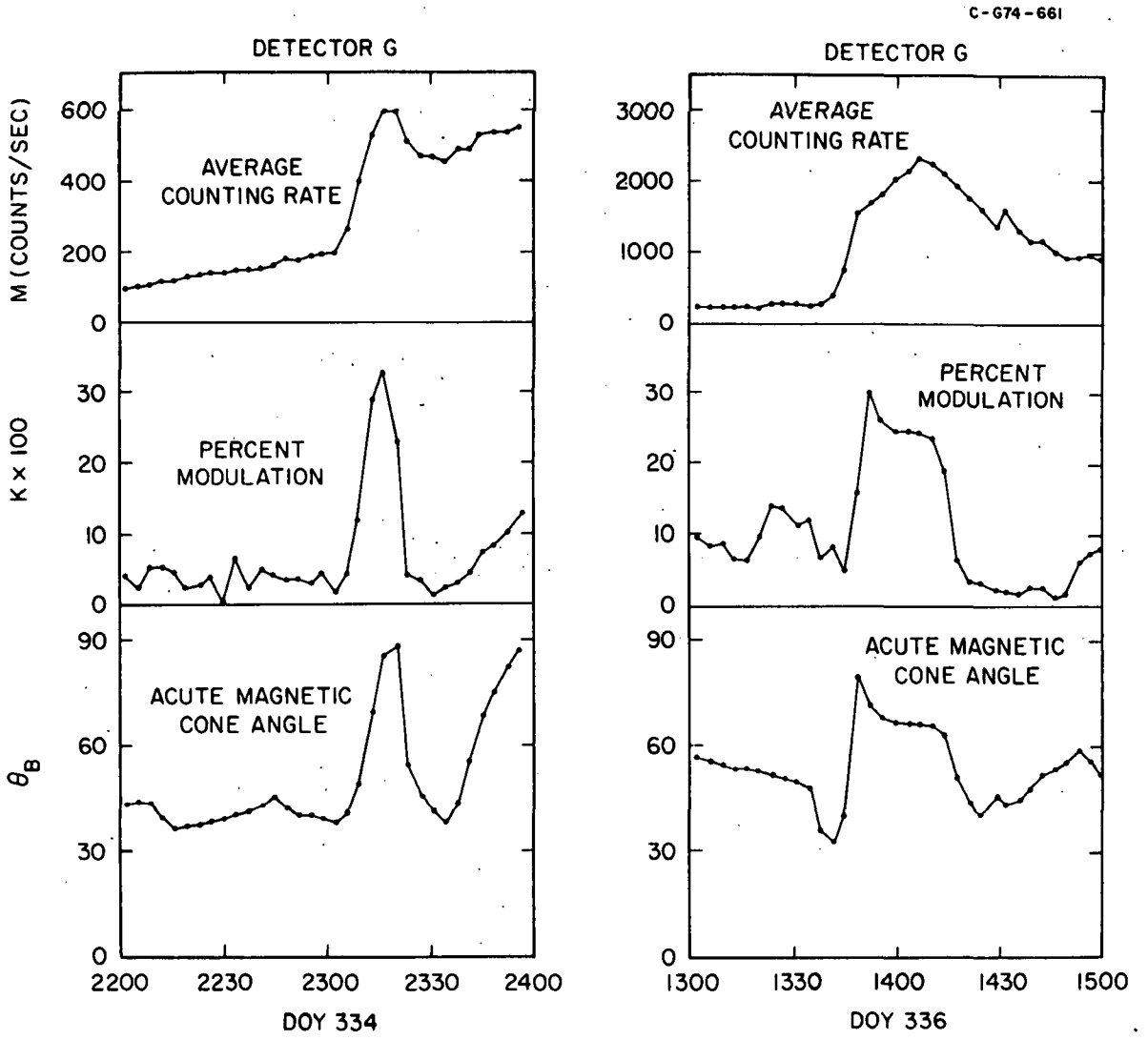
C-G74-661
DETECTOR G
AVERAGE COUNTING RATE
M (COUNTS/SEC)
600
400
200
0
PERCENT MODULATION
K x 100
30
20
10
0
ACUTE MAGNETIC CONE ANGLE
θ_B
90
60
30
0
2200
2230
2300
2330
2400
DOY 334
DETECTOR G
AVERAGE COUNTING RATE
3000
2000
1000
0
PERCENT MODULATION
30
20
10
0
ACUTE MAGNETIC CONE ANGLE
90
60
30
0
1300
1330
1400
1430
1500
DOY 336

Figure 8

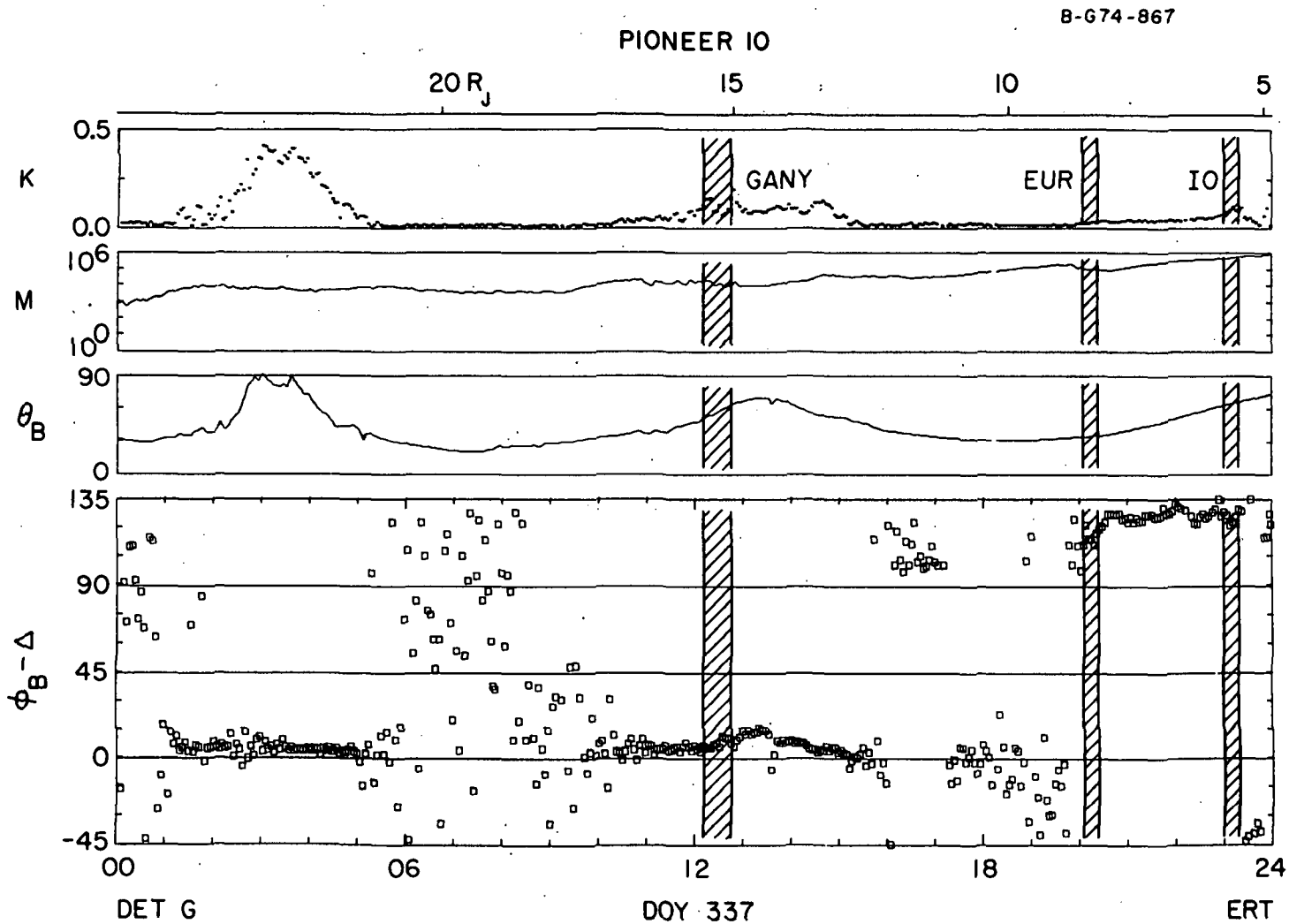
B-G74-867
PIONEER 10
20 R_J
15
10
5
K
0.5
0.0
GANY
EUR
IO
M
10^6
10^0
θ_B
90
0
φ_B - Δ
135
90
45
0
-45
00
06
12
18
24
DET G
DOY 337
ERT

Figure 9

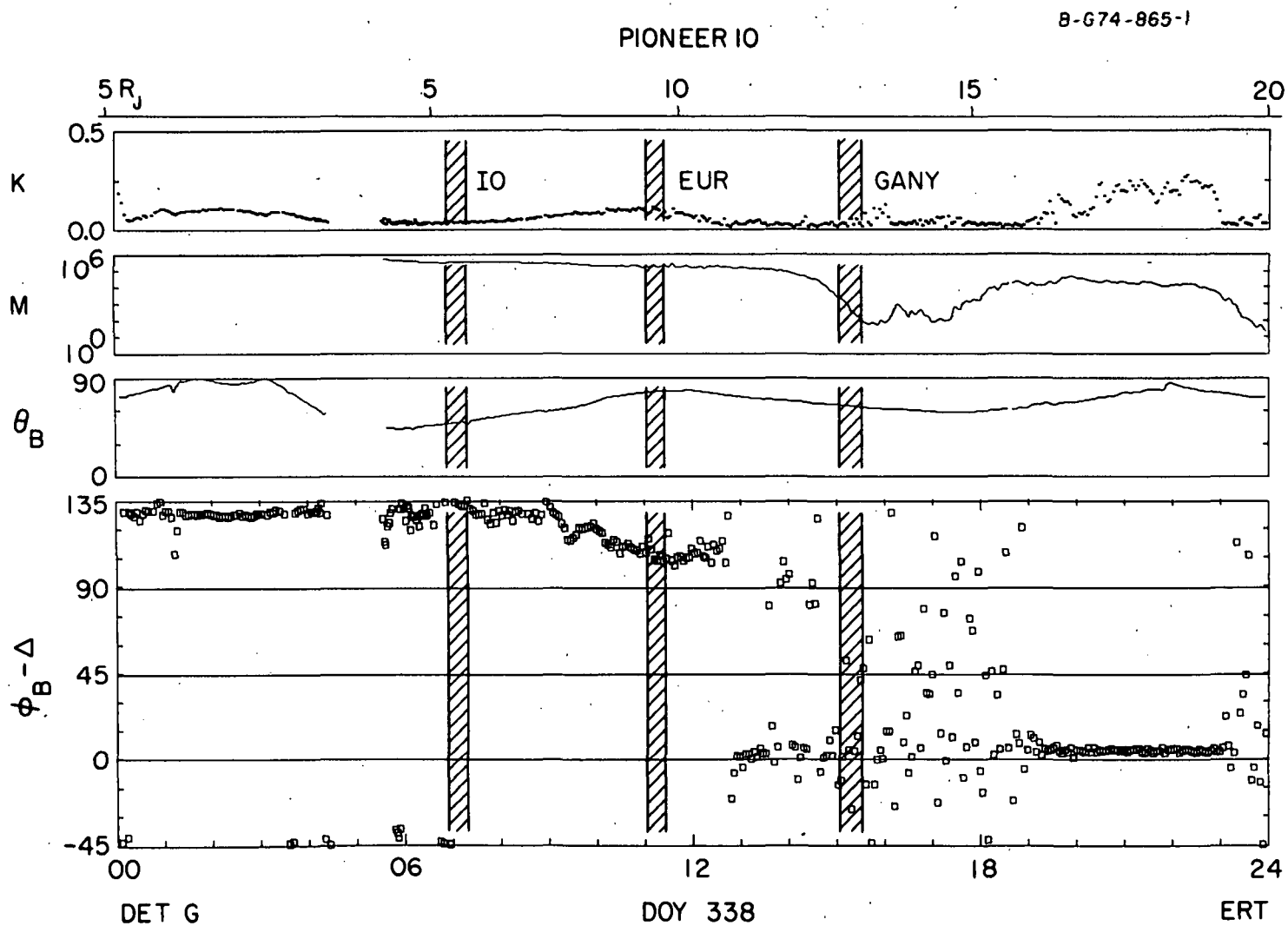
B-G74-865-1
PIONEER 10
5 R_J
5
10
15
20
0.5
K
0.0
IO
EUR
GANY
10^6
M
10^0
90
θ_B
0
135
90
φ_B - Δ
45
0
-45
00
06
12
18
24
DET G
DOY 338
ERT

Figure 10

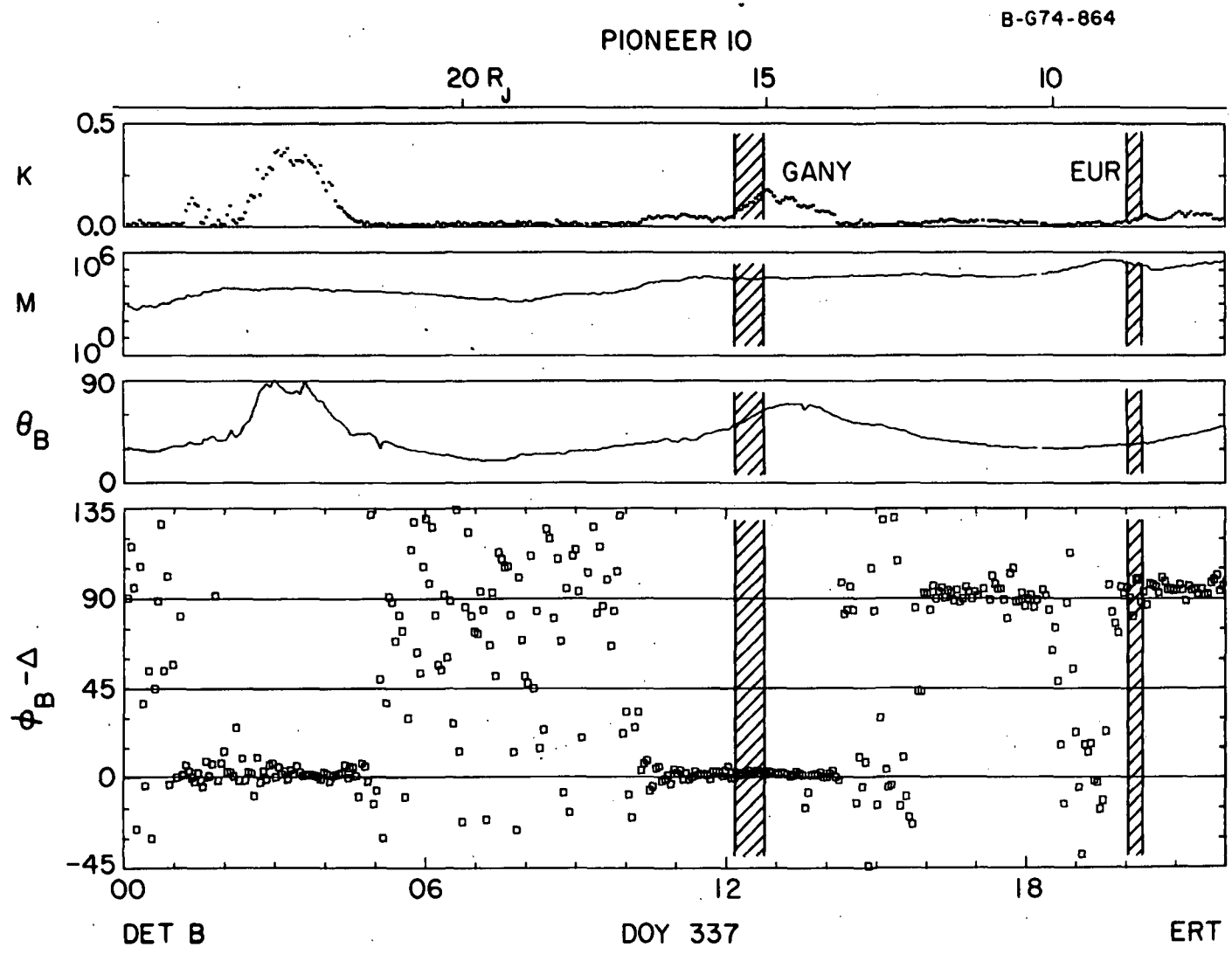
B-G74-864
PIONEER 10
20 R_J
15
10
K
0.5
0.0
GANY
EUR
M
10^6
10^0
θ_B
90
0
φ_B - Δ
135
90
45
0
-45
00
06
12
18
DET B
DOY 337
ERT

Figure 11

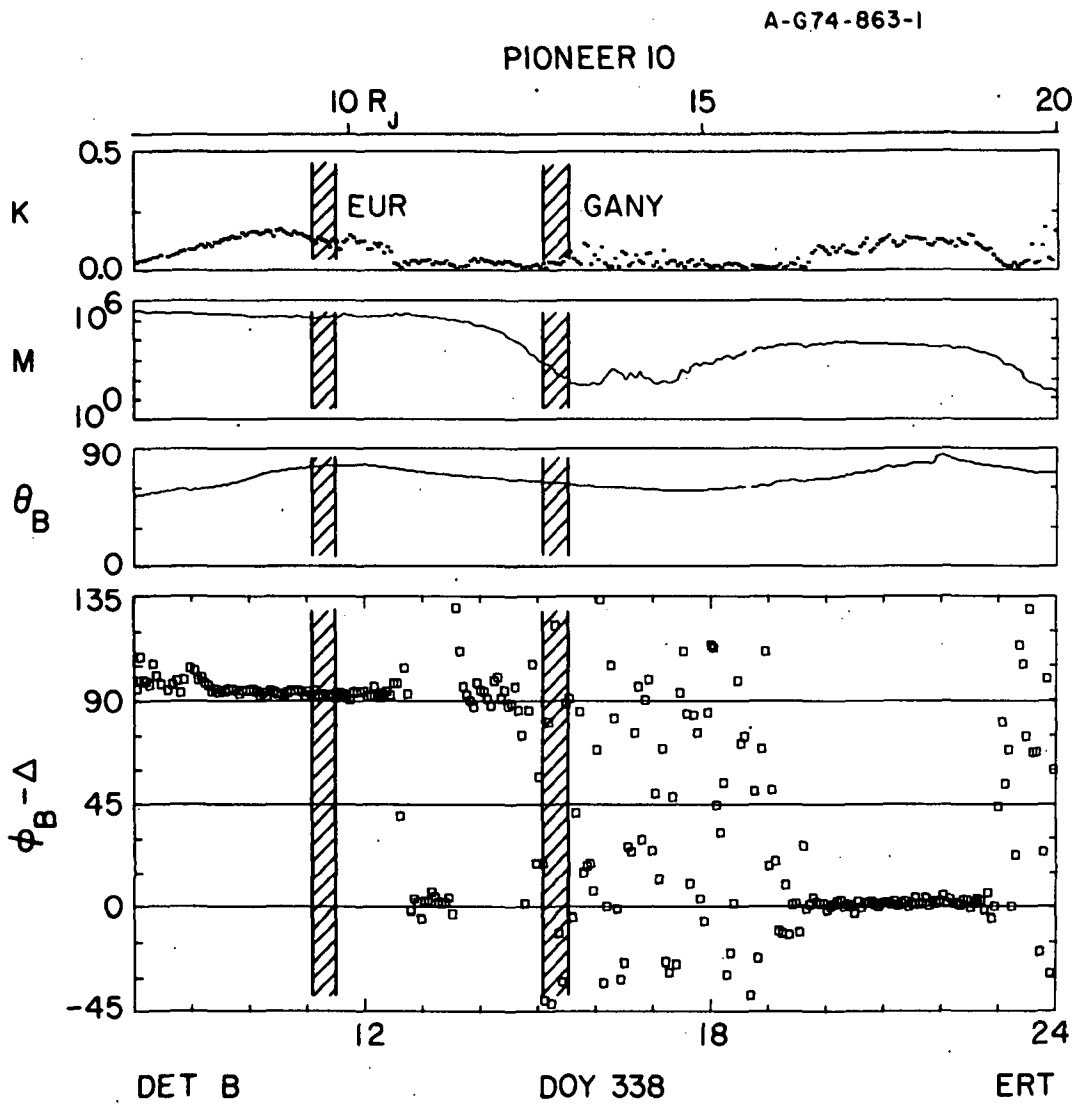
A-G74-863-1
PIONEER 10
10 R_J
15
20
0.5
0.0
K
EUR
GANY
10^6
10^0
M
90
0
θ_B
135
90
45
0
-45
φ_B - Δ
12
18
24
DET B
DOY 338
ERT

Figure 12

D-G74-326

PIONEER 10 ENCOUNTER
MAGNETIC MERIDIAN PLANE PROJECTION

CENTERED DIPOLE { TILT = 9.5°
λ_{III} (1957) = 230°

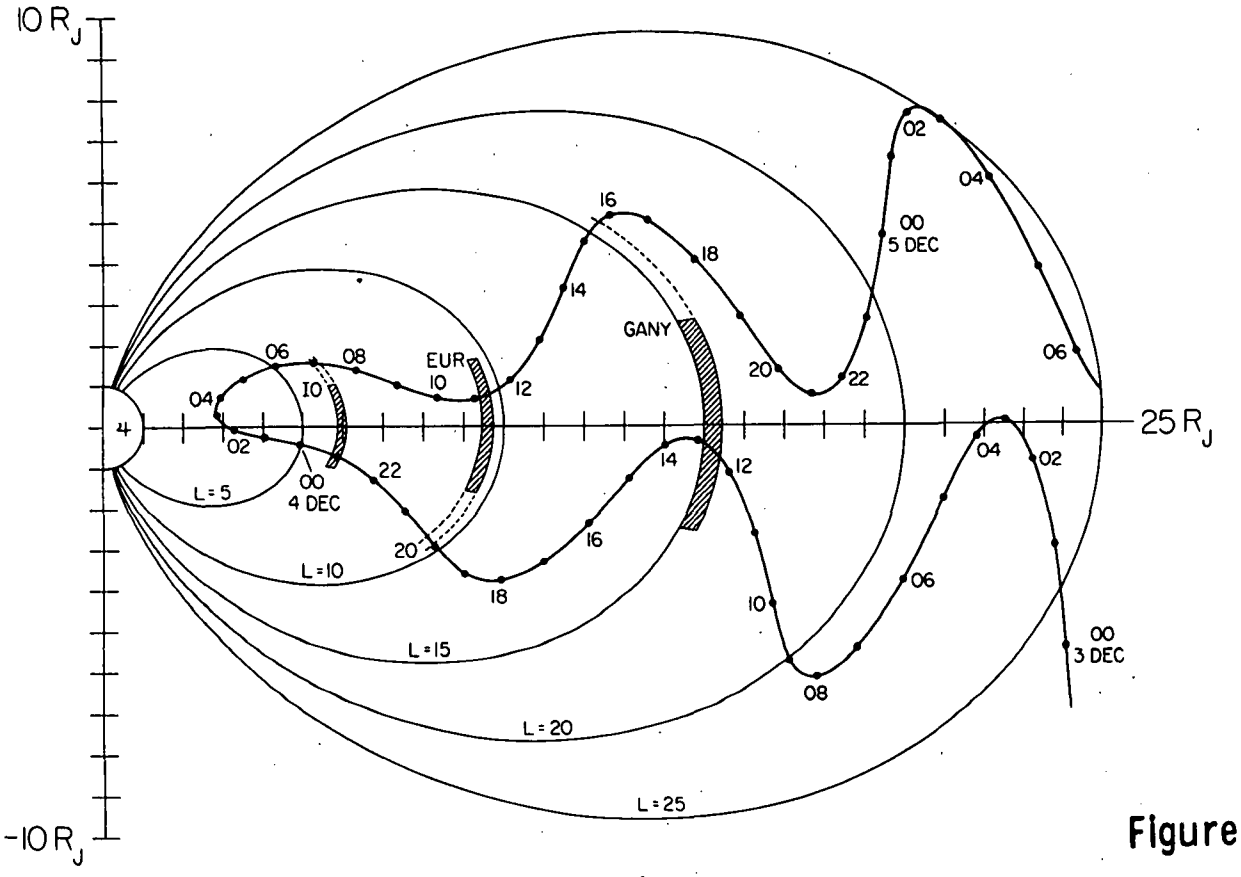

Figure 13